Inorg. Chem. **2006**, *45*, 1059–1068

Synthesis, Structural Characterization, and Theoretical Studies of Gold(I) and Gold(I)–Gold(III) Thiolate Complexes: Quenching of Gold(I) Thiolate Luminescence

Manuel Bardají,*[†,‡,§] Maria José Calhorda,[||] Paulo J. Costa,[||] Peter G. Jones,[⊥] Antonio Laguna,*[,‡] M. Reyes Pérez,[‡] and M. D. Villacampa[‡]

Química Inorgánica, Facultad de Ciencias, Universidad de Valladolid, E-47005 Valladolid, Spain, Departamento de Química Inorgánica, Instituto de Ciencia de Materiales de Aragón, Universidad de Zaragoza-CSIC, E-50009 Zaragoza, Spain, Departamento de Química e Bioquímica, Faculdade de Ciências, Universidade de Lisboa, Campo Grande 1749-016 Lisboa, Portugal, and ITQB, Avenida da República, EAN, Apartado 127, 2781-901, Oeiras, Portugal, and Institut für Anorganische und Analytische Chemie der Technischen Universität, Postfach 3329, D-38023 Braunschweig, Germany

Received July 13, 2005

The gold(I) thiolate complexes $[Au(2\text{-}SC_6H_4NH_2)(PPh_3)]$ (**1**), $[PPN][Au(2\text{-}SC_6H_4NH_2)_2]$ (**2**) (PPN = $PPh_3{=}N{=}PPh_3$), and $[\{Au(2\text{-}SC_6H_4NH_2)\}_2(\mu\text{-dppm})]$ (**3**) (dppm = $PPh_2CH_2PPh_2$) have been prepared by reaction of acetylacetonato gold(I) precursors with 2-aminobenzenethiol in the appropriate molar ratio. All products are intensely photoluminescent at 77 K. The molecular structure of the dinuclear derivative **3** displays a gold–gold intramolecular contact of 3.1346(4) Å. Further reaction with the organometallic gold(III) complex $[Au(C_6F_5)_3(tht)]$ affords dinuclear or tetranuclear mixed gold(I)–gold(III) derivatives with a thiolate bridge, namely, $[(AuPPh_3)\{Au(C_6F_5)_3\}(\mu_2\text{-}2\text{-}SC_6H_4NH_2)]$ (**4**) and $[(C_6F_5)_3Au(\mu_2\text{-}2\text{-}SC_6H_4NH_2)(AudppmAu)(\mu_2\text{-}2\text{-}SC_6H_4NH_2)Au(C_6F_5)_3]$ (**5**). X-ray diffraction studies of the latter show a shortening of the intramolecular gold(I)–gold(I) contact [2.9353(7) or 2.9332(7) Å for a second independent molecule], and short gold(I)–gold(III) distances of 3.2812(7) and 3.3822(7) Å [or 3.2923(7) and 3.4052(7) Å] are also displayed. Despite the gold–gold interactions, the mixed derivatives are nonemissive compounds. Therefore, the complexes were studied by DFT methods. The HOMOs and LUMOs for gold(I) derivatives **1** and **3** are mainly centered on the thiolate and phosphine (or the second thiolate for complex **2**), respectively, with some gold contributions, whereas the LUMO for derivative **4** is more centered on the gold(III) fragment. TD-DFT results show a good agreement with the experimental UV–vis absorption and excitation spectra. The excitations can be assigned as a S → Au–P charge transfer with some mixture of LLCT for derivative **1**, an LLCT mixed with ILCT for derivative **2**, and a S → Au···Au–P charge transfer with LLCT and MC for derivative **3**. An LMCT (thiolate → Au^{III} mixed with thiolate → Au–P) excitation was found for derivative **4**. The differing nature of the excited states [participation of the gold(III) fragment and the small contribution of sulfur] is proposed to be responsible for quenching the luminescence.

Introduction

There has long been an interest in the synthesis of derivatives containing the P−Au(I)−S unit because they are related to Auronafin, a drug used against rheumatoid arthritis.[1] Moreover, closed-shell gold(I) complexes usually display gold(I)−gold(I) interactions, which have been attributed to correlation effects reinforced by relativistic effects and electrostatic contributions.[2,3] In contrast, gold(I)−gold(III) interactions are rare and have been reported only for

* To whom correspondence should be addressed. E-mail: bardaji@qi.uva.es (M.B.), alaguna@unizar.es (A.L.). Fax: + 34 983423013 (M.B.), + 34 976761187 (A.L.).

[†] Universidad de Valladolid.

[‡] Universidad de Zaragoza-CSIC.

[§] Present and permanent address: Química Inorgánica, Facultad de Ciencias, Universidad de Valladolid, E-47005 Valladolid, Spain.

[||] Universidade de Lisboa and ITQB.

[⊥] Institut für Anorganische und Analytische Chemie der Technischen Universität.

(1) Shaw, C. F., III. *Gold: Progress in Chemistry, Biochemistry, and Technology*; Schmidbaur, H., Ed.; John Wiley & Sons: Chichester, U.K., 1999; p 259.

(2) Pyykkö, P. *Chem. Rev.* **1997**, *97*, 597.

(3) Runeberg, N.; Schütz, M.; Werner, H. J. *J. Chem. Phys.* **1999**, *110*, 7210.

10.1021/ic051168u CCC: $33.50
Published on Web 01/12/2006

some doubly bridged ylide complexes[4−7] and sulfide,[8,9] thiolate,[10] or selenide[11] mixed derivatives.

Recently, luminescent gold(I) complexes have been reported in which the P-donor ligand is a tertiary mono-, di-, or triphosphine and the S-donor ligand is a thiolate or dithiolate.[12−20] The emission occurs over a wide range (ca. 400−700 nm) and has usually been assigned to a thiolate-to-gold charge-transfer excited state, sometimes complicated by the presence of gold−gold interactions and ascribed to a thiolate-to-gold−gold charge transfer. Thiolate-to-phosphine charge-transfer, gold-to-thiolate charge-transfer,[21] or even thiolate-centered transitions have also been suggested.[15] Moreover, Yam and co-workers have designed diphosphine-thiolate gold(I) complexes able to bind specifically to various metal cations.[15,22,23]

Zhang and co-workers have modeled several dinuclear complexes with a dithiolate and a mono- or diphosphine ligand to study both the luminescent properties and the aurophilicity of the parent compounds. Their results, based on correlated methods, revealed that both gold(I)−gold(I) interactions and the dithiolate ligand are clearly involved in the emission. They therefore assigned the emission to a thiolate-to-gold−gold charge-transfer excited state.[24,25]

In this article, we report the synthesis of mono- and dinuclear gold(I) thiolate complexes that are intensely emissive at low temperature in the solid state. The dinuclear derivative with a bridging diphosphine exhibits a short gold−gold contact. Di- or tetranuclear mixed gold(I)−gold(III) thiolate derivatives are obtained by reaction with an organometallic gold(III) complex, affording nonemissive derivatives, although the molecular structure of the tetranuclear complex maintains the short gold(I)−gold(I) distances and additionally displays short gold(I)−gold(III) contacts. To understand the photophysical properties in the gold(I) and gold(I)−gold(III) complexes, DFT calculations were carried out to determine the frontier orbitals and to assign the electronic transitions.

Experimental Section

General. All reactions were carried out under an argon atmosphere at room temperature. IR spectra were recorded on a Perkin-Elmer 883 spectrophotometer, over the range 4000−200 cm^{-1} using Nujol mulls between polyethylene sheets. ^1H, ^{19}F, and $^{31}P\{^1H\}$ NMR spectra were recorded on a Bruker ARX·300 or GEMINI 2000 apparatus in $CDCl_3$ solution (if no other solvent is stated); chemical shifts are quoted relative to $SiMe_4$ (external, ^1H), $CFCl_3$ (external, ^{19}F) and 85% H_3PO_4 (external, ^{31}P). C, H, N, and S analyses were performed with a Perkin-Elmer 2400 microanalyzer. Mass spectra were recorded on a VG Autospec instrument using the FAB technique (with a Cs gun) and 3-nitrobenzyl alcohol as the matrix. Emission and excitation spectra were measured in the solid state as finely pulverized KBr mixtures at room temperature and 77 K with a Perkin-Elmer LS-55 spectrofluorometer. UV−vis absorption spectra in dichloromethane solution were recorded at 298 K on a Shimadzu UV-1603 spectrometer.

Preparation of [Au(2-$SC_6H_4NH_2$)(PPh_3)] (1). To a dichloromethane solution (20 mL) of 2-aminobenzenethiol (29 μL, 0.27 mmol) was added [Au(acac)(PPh_3)][26] (150 mg, 0.27 mmol), and the mixture was stirred for about 1 h. The solution was concentrated to ca. 2 mL, and the addition of hexane afforded **1** as a white solid. Yield of **1**: 130 mg, 83%. ^1H NMR: δ 4.40 (s, 2H, NH_2), 6.59 (td, 1H, J_{HH} = 7.4 and 1.3 Hz, C_6H_4), 6.70 (dd, 1H, J_{HH} = 7.7 and 1.3 Hz, C_6H_4), 6.90 (td, 1H, J_{HH} = 7.5 and 1.3 Hz, C_6H_4), 7.4−7.5 (m, 15H, Ph), 7.61 (dd, 1H, J_{HH} = 7.7 and 1.5 Hz, C_6H_4). $^{31}P\{^1H\}$ NMR: δ 38.6 (s). IR: 3442 [m, ν(N−H)], 3340 [m, ν(N−H)], 1602 [s, δ(N−H)] cm^{-1}. Anal. Calcd for $C_{24}H_{21}AuNPS$: C, 49.4; H, 3.65; N, 2.4; S, 5.5. Found: C, 49.7; H, 3.8; N, 2.45; S, 5.2. FAB^+ (*m*/*z*, %, assignment): 459 (100, $[AuPPh_3]^+$), 583 (20, $[M]^+$), 1042 (47 $[M + AuPPh_3]^+$).

Preparation of [PPN][Au(2-$SC_6H_4NH_2$)$_2$] (2). To 20 mL of a dichloromethane solution of 2-aminobenzenethiol (22 μL, 0.2 mmol) was added [PPN][Au(acac)$_2$][27] (93 mg, 1 mmol), and the mixture was stirred for about 2 h. The solvent was removed, and the white residue was washed with petroleum ether. Yield of **2**: 69 mg, 70%. ^1H NMR: δ 4.33 (s, 4H, NH_2), 6.39 (t, 2H, J_{HH} = 7.5 Hz, C_6H_4), 6.50 (d, 2H, J_{HH} = 7.8 Hz, C_6H_4), 6.68 (t, 2H, J_{HH} = 7.2 Hz, C_6H_4), 7.4−7.6 (m, 32H, Ph + C_6H_4). $^{31}P\{^1H\}$ NMR: δ 21.8 (s, PPh_3═N═PPh_3). IR: 3446 [w, ν(N−H)], 3319 [w, ν(N−H)], 1596 [s, δ(N−H)] cm^{-1}. Anal. Calcd for $C_{48}H_{42}AuN_3P_2S_2$: C, 58.6; H, 4.3; N, 4.25; S, 6.5. Found: C, 58.3; H, 4.2; N, 4.35; S, 6.2. FAB^- (*m*/*z*, %, assignment): 445 (100, [M-PPN]$^-$).

Preparation of [{Au(2-$SC_6H_4NH_2$)}$_2$(μ-dppm)] (3). To a dichloromethane solution (20 mL) of 2-aminobenzenethiol (11 μL, 0.1 mmol) was added [{Au(acac)}$_2$(μ-dppm)] (98 mg, 0.1 mmol; prepared as for PPh_3 in ref 26), and the mixture was stirred for

(4) Mazany, A. M.; Fackler, J. P., Jr. *J. Am. Chem. Soc.* **1984**, *106*, 801.
(5) Fackler, J. P., Jr.; Trzcinska-Bancroft, B. *Organometallics* **1985**, *4*, 1891.
(6) Schmidbaur, H.; Hartmann, C.; Reber, G.; Müller, G. *Angew. Chem., Int. Ed. Engl.* **1987**, *26*, 1146.
(7) Raptis, R. G.; Porter, L. C.; Emrich, R. J.; Murray, H. H.; Fackler, J. P., Jr. *Inorg. Chem.* **1990**, *29*, 4408.
(8) Canales, F.; Gimeno, M. C.; Laguna, A.; Jones, P. G. *Organometallics* **1996**, *15*, 3412.
(9) Calhorda, M. J.; Canales, F.; Gimeno, M. C.; Jiménez, J.; Jones, P. G.; Laguna, A.; Veiros, L. F. *Organometallics* **1997**, *16*, 3837.
(10) Crespo, O.; Canales, F.; Gimeno, M. C.; Jones, P. G.; Laguna, A. *Organometallics* **1999**, *18*, 3142.
(11) Canales, S.; Crespo, O.; Gimeno, M. C.; Jones, P. G.; Laguna, A.; Mendizabal, F. *Organometallics* **2001**, *20*, 4812.
(12) Jones, W. B.; Yuan, J.; Narayanaswamy, R.; Young, M. A.; Elder, R. C.; Bruce, A. E.; Bruce M. R. M. *Inorg. Chem.* **1995**, *34*, 1996.
(13) Forward, J. M.; Bohmann, D.; Fackler, J. P. Jr.; Staples, R. J. *Inorg. Chem.* **1995**, *34*, 6330.
(14) Tang, S. S.; Chang, C.; Lin, I. J. B.; Liou, L.; Wang, J. *Inorg. Chem.* **1997**, *36*, 2294.
(15) Yam, V. W. W.; Chan, C. L.; Li, C. K.; Wong, K. M. C. *Coord. Chem. Rev.* **2001**, *216−217*, 173.
(16) Bardají, M.; Laguna, A.; Vicente, J.; Jones, P. G. *Inorg. Chem.* **2001**, *40*, 2675.
(17) Bardají, M.; Laguna, A.; Pérez, M. R.; Jones, P. G. *Organometallics* **2002**, *21*, 1877.
(18) Vicente, J.; González-Herrero, P.; García-Sánchez, Y.; Jones, P. G.; Bardají, M. *Inorg. Chem.* **2004**, *43*, 7516.
(19) Bardají, M.; de la Cruz, M. T.; Jones, P. G.; Laguna, A.; Martínez, J.; Villacampa, M. D. *Inorg. Chim. Acta* **2005**, *358*, 1365.
(20) Chen J. H.; Mohamed A. A.; Abdou H. E.; Bauer J. A. K.; Fackler J. P.; Bruce A. E.; Bruce M. R. M. *Chem. Commun.* **2005**, 1575.
(21) Watase, S.; Nakamoto, M.; Kitamura, T.; Kanehisa, N.; Kai, Y.; Yanagida, S. *J. Chem. Soc., Dalton Trans.* **2000**, 3585.
(22) Yam, V. W. W.; Li, C. K.; Chan, C. L. *Angew. Chem., Int. Ed.* **1998**, *37*, 2857.
(23) Li, C. K.; Lu, X. X.; Wong, K. M. C.; Chan, C. L.; Zhu, N.; Yam, V. W. W. *Inorg. Chem.* **2004**, *43*, 7421.
(24) Pan, Q. J.; Zhang, H. X. *Eur. J. Inorg. Chem.* **2003**, *23*, 4202.
(25) Pan, Q. J.; Zhang, H. X. *Organometallics* **2004**, *23*, 5198.
(26) Vicente, J.; Chicote, M. T. *Inorg. Synth.* **1998**, *32*, 175.
(27) Vicente, J.; Chicote, M. T.; Saura-Llamas, I.; Lagunas, M. C. *Chem. Commun.* **1992**, 915.

Table 1. Details of Crystal Data and Structure Refinement for Complexes **3** and **5**

	3	**5**
empirical formula	$C_{37}H_{34}Au_2N_2P_2S_2$	$C_{73}H_{34}Au_4F_{30}N_2P_2S_2$
formula weight	1026.66	2422.95
temperature	100(2) K	133(2) K
wavelength	0.71073 Å	0.71073 Å
crystal system	monoclinic	orthorhombic
space group	$P2_1/c$	$Pca2_1$
unit cell dimensions	$a = 11.5662(9)$ Å	$a = 22.864(2)$ Å
	$b = 11.2001(8)$ Å	$b = 30.371(2)$ Å
	$c = 26.757(2)$ Å	$c = 24.697(2)$ Å
	$\alpha = 90°$	$\alpha = 90°$
	$\beta = 91.870(1)°$	$\beta = 90°$
	$\gamma = 90°$	$\gamma = 90°$
volume	3464.3(4) Å^3	17150(2) Å^3
Z	4	8
density (calcd)	1.968 Mg/m^3	1.877 Mg/m^3
absorption coefficient	8.703 mm^{-1}	7.012 mm^{-1}
F(000)	1960	8976
crystal habit	colorless needle	colorless tablet
crystal size	0.2 × 0.08 × 0.08 mm	0.31 × 0.22 × 0.08 mm
θ range for data collection	1.76−28.78°	0.67−28.30°
index ranges	$-12 \le h \le 15$, $-15 \le k \le 14$,	$-30 \le h \le 30$, $-40 \le k \le 40$,
	$-35 \le l \le 33$	$-32 \le l \le 32$
reflections collected	22494	275207
independent reflections	8133 [R(int) = 0.0870]	42596 [R(int) = 0.0953]
absorption correction	SADABS	SADABS
max and min transmission	1.000 and 0.565	0.746 and 0.483
refinement method	full-matrix least-squares on F^2	full-matrix least-squares on F^2
data/restraints/parameters	8133/0/406	42596/337/1318
GOF on F^2	0.880	1.057
final R indices [$I > 2\sigma(I)$]	R1 = 0.0446, wR2 = 0.0812	R1 = 0.0446, wR2 = 0.1134
R indices (all data)	R1 = 0.0675, wR2 = 0.0873	R1 = 0.1001, wR2 = 0.1390
largest diff peak and hole	2.324 and −1.421 e.Å^{-3}	3.067 and −1.732 e. Å^{-3}

about 1 h. The solution was concentrated to ca. 2 mL, and the addition of hexane afforded **3** as a yellow solid. Yield of **3**: 85 mg, 83%. ^{1}H NMR: δ 3.69 (t, 2H, ^2J = 11.2 Hz, CH_2P), 4.50 (s, 4H, NH_2), 6.55 (t, 2H, J_{HH} = 7.3 Hz, C_6H_4), 6.68 (d, 2H, J_{HH} = 8.2 Hz, C_6H_4), 6.92 (t, 2H, J_{HH} = 7.3 Hz, C_6H_4), 7.2−7.6 (m, 22H, Ph + C_6H_4). ^{31}P{^{1}H} NMR: δ 29.2 (s). IR: 3400 [m, br, ν(N−H)], 1605 [s, δ(N−H)] cm^{-1}. Anal. Calcd for $C_{37}H_{34}Au_2N_2P_2S_2$: C, 43.3; H, 3.35; N, 2.75; S, 6.25. Found: C, 43.4; H, 3.35; N, 2.45; S, 6.1. FAB$^+$ (*m*/*z*, %, assignment): 902 (100, [M − $SC_6H_4NH_2$]$^+$), 1223 (37, [M + Au]$^+$).

Preparation of [(AuPPh$_3$){Au(C$_6$F$_5$)$_3$}(μ_2-2-SC$_6$H$_4$NH$_2$)] (4) and [(C$_6$F$_5$)$_3$Au(μ_2-2-SC$_6$H$_4$NH$_2$)(AudppmAu)(μ_2-2-SC$_6$H$_4$NH$_2$)-Au(C$_6$F$_5$)$_3$] (5). To a dichloromethane solution (20 mL) of **1** (58 mg, 0.1 mmol) or **3** (51 mg, 0.05 mmol) was added [Au(C$_6$F$_5$)$_3$(tht)][28] (tht = tetrahydrothiophene; 79 mg, 0.1 mmol). After being stirred for 2 h, the solution was concentrated to ca. 3 mL. Addition of hexane afforded complex **4** or **5**, respectively, as a white (**4**) or yellow (**5**) solid. Yield of **4**: 96 mg, 75%. ^{1}H NMR: δ 4.23 (s, 2H, NH_2), 6.42 (t, 1H, J_{HH} = 7.5 Hz, C_6H_4), 6.49 (d, 1H, J_{HH} = 8.0 Hz, C_6H_4), 6.93 (t, 1H, J_{HH} = 7.6 Hz, C_6H_4), 7.36 (d, 1H, J_{HH} = 7.8 Hz, C_6H_4), 7.5−7.6 (m, 15H, Ph). ^{19}F NMR δ −120.72 (m, 4F$_o$), −122.83 (m, 2F$_o$), −158.85 (t, $^3J_{FF}$ = 20.0 Hz, 1F$_p$), −159.20 (t, $^3J_{FF}$ = 20.1 Hz, 2F$_p$), −162.46 (m, 4F$_m$), −162.93 (m, 2F$_m$). ^{31}P{^{1}H} NMR: δ 37.1 (s). IR: 3477 [w, ν(N−H)], 3390 [w, ν-(N−H)], 1638 [w, δ(N−H)], 1615 [s, δ(N−H)], 967 (s), 805 (s), 794 (s) cm^{-1} from the C_6F_5 group. Anal. Calcd for $C_{42}H_{21}Au_2F_{15}$-NPS: C, 39.35; H, 1.65; N, 1.1; S, 2.5. Found: C, 39.7; H, 1.95; N, 1.15; S, 2.2. FAB$^+$ (*m*/*z*, %, assignment): 459 (100, [Au-(PPh$_3$)]$^+$), 583 (85, [M − Au(C$_6$F$_5$)$_3$]$^+$), 1114 (27, [M − C$_6$F$_5$]$^+$), 1281 (11, [M]$^+$). Yield of **5**: 103 mg, 85%. ^{1}H NMR: δ 3.74 (t, 2H, ^2J = 11.2 Hz, CH_2P), 4.09 (s, 4H, NH_2), 5.63 (t, 2H, J_{HH} = 7.2 Hz, C_6H_4), 6.46 (d, 2H, J_{HH} = 8.0 Hz, C_6H_4), 6.51 (d, 2H, J_{HH} = 7.6 Hz, C_6H_4), 6.74 (t, 2H, J_{HH} = 7.3 Hz, C_6H_4), 7.5−7.7 (m, 20H, Ph). ^{19}F NMR δ −121.05 (m, 4F$_o$), −122.93 (m, 2F$_o$), −158.73 (t, $^3J_{FF}$ = 20.1 Hz, 1F$_p$), −158.93 (t, $^3J_{FF}$ = 20.1 Hz, 2F$_p$), −162.27 (m, 4F$_m$), −162.87 (m, 2F$_m$). ^{31}P{^{1}H} NMR: δ 33.8 (s). IR: 3460 [w, ν(N−H)], 3360 [w, ν(N−H)], 1620 [m, δ(N−H)], 970 (s), 807 (s), 797 (s) cm^{-1} from the C_6F_5 group. Anal. Calcd for $C_{73}H_{34}Au_4F_{30}N_2P_2S_2$: C, 36.2; H, 1.4; N, 1.15; S, 2.65. Found: C, 35.9; H, 1.45; N, 1.1; S, 2.3. FAB$^+$ (*m*/*z*, %, assignment): 902 (100, [M − 2(Au(C$_6$F$_5$)$_3$) − $SC_6H_4NH_2$]$^+$), 1432 (22, [M − Au(C$_6$F$_5$)$_3$ − C$_6$F$_5$ − H]$^+$), 1600 (19, [M − Au(C$_6$F$_5$)$_3$ − $SC_6H_4NH_2$]$^+$).

Crystal Structure Determination of Derivatives 3 and 5. The crystals were mounted in inert oil on glass fibers and transferred to the cold gas stream of a Bruker SMART CCD diffractometer. Crystal data and details of data collection and structure refinement are given in Table 1. Absorption corrections were based on multiple scans (program SADABS). The structures were refined anisotropically on F^2 using the program SHELXL-97.[29] For complex **3**, all non-hydrogen atoms were refined anisotropically, and hydrogen atoms were included using a riding model. Special details of refinement for **5**: The structure is pseudosymmetric[30] (the maximum deviations from the corresponding centrosymmetric space group are only ca. 0.7 Å) and was refined as an enantiomorphic twin. The twinning parameter refined to 0.378(7). Note that a value of 0.5 would be expected if the structure were actually centrosymmetric. The C and N atoms were refined isotropically. Several significant difference peaks were observed, presumably corresponding to solvent of crystallization, but could not be connected to form any sensible molecule. Arbitrarily, two were refined as chlorine and five as carbon. None of these atoms was taken into account in

(28) Usón, R.; Laguna, A.; Laguna, M. *Inorg. Synth.* **1989**, *26*, 87.

(29) Sheldrick, G. M. *SHELXL 97: A Program for Crystal Structure Refinement*; University of Göttingen: Göttingen, Germany, 1997.

calculating the molecular weight and other composition-related parameters. The aminic hydrogens were not located.

DFT Calculations. Density functional theory (DFT) calculations[31] were carried out with the Amsterdam Density Functional (ADF 2004.01) program.[32] The Vosko, Wilk, and Nusair local exchange correlation potential was used.[33] Gradient-corrected geometry optimizations[34] were performed, using the generalized gradient approximation (Perdew−Wang nonlocal exchange and correlation corrections, PW91[35]). Relativistic effects were treated with the ZORA approximation.[36] The core orbitals were frozen for Au [(1−4)s, (2−4)p, (3−4)d]; P; S [(1−2)s, 2p]; and C, N, and F (1s). Triple-ζ Slater-type orbitals (STOs) were used to describe the valence shells of C, O (2s and 2p), P (3s, 3p), and Au (4f, 5d, 6s). A set of two polarization functions was added to each C, O (single-ζ, 3d, 4f), P, S (single-ζ, 3d, 4p), and Au (single-ζ, 6p, 5f). Triple-ζ Slater-type orbitals (STOs) were used to describe the valence shells of H (1s) with one polarization function (single-ζ, 2p). Full geometry optimizations were performed without any symmetry constraints on complexes based on the crystal structures described below. Time-dependent DFT calculations (TD-DFT)[37] in the ADF implementation were used to determine the excitation energies. Mayer indices[38] were calculated with the ADF densities using the MAYER program[39] and were used as bond strength indicators. Three-dimensional representations of orbitals were obtained with Molekel.[40]

Results and Discussion

Synthesis and Characterization. We have carried out reactions of 2-aminobenzenethiol with acetylacetonato derivatives of gold(I), which are able to deprotonate the thiol. The resulting thiolate coordinates to the corresponding gold(I) fragment, as a result of the loss of the protonated acac ligand; this is known as the "acac method".[41] The corresponding gold thiolate derivatives **1**−**3** were regioselectively obtained, according to Scheme 1. Schmidbaur and coworkers reported the regioselective double auration to afford the sulfonium complex $[(2\text{-}H_2NC_6H_4)S(AuPPh_3)_2]BF_4$.[42]

Scheme 1[a]

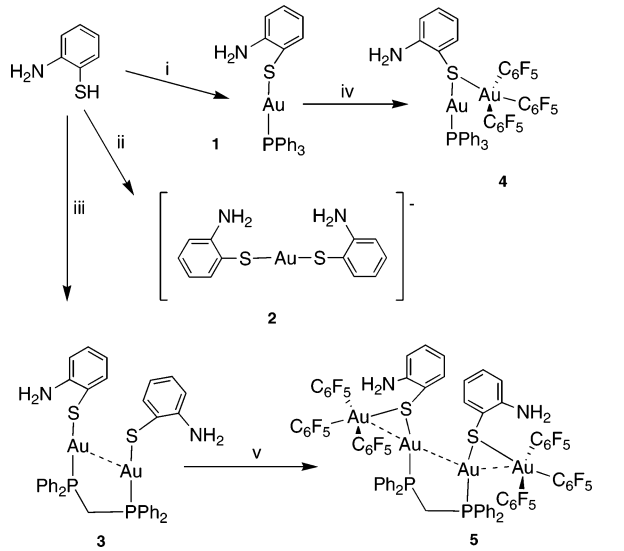

[a] (i) [Au(acac)(PPh$_3$)], (ii) [PPN][Au(acac)$_2$], (iii) [{Au(acac)}$_2$(μ-dppm)], (iv) [Au(C$_6$F$_5$)$_3$(tht)], (v) 2[Au(C$_6$F$_5$)$_3$(tht)].

These derivatives are air- and moisture-stable white (**1** and **2**) or yellow (**3**) solids at room temperature. They were readily characterized by elemental analysis and mass, IR, and NMR spectroscopies. The addition of an excess of [Au(acac)(PPh$_3$)] does not produce further reaction, and the monosubstituted derivative is always obtained. More gold fragments can be introduced into such derivatives using the N-donor atom, as found in the mononuclear gold(III) derivative $[Au(\kappa C^1,\kappa N,2\text{-}NMe_2CH_2C_6H_4)(\kappa N,\kappa S,2\text{-}SC_6H_4\text{-}NH_2)](ClO_4)$,[43] by forming unsupported gold−gold interactions, as found for $[\{(pta)_3Au^I\}_2Au^I_2(i\text{-}mnt)_2]$ (i-mnt = isomalononitriledithiolate, pta = phosphatriazaadamantane)[44] and $[\{(C_6F_5)_3Au^{III}\}Au^I_2(CH_2PPh_2CH_2)_2]$,[45] or, more typically, the S-donor atom to give derivatives as reported for other thiolato derivatives such as $[RS(AuL)_n]^{(n-1)+}$ (L = phosphine, $n = 1-3$)[46] and $[(C_6F_5)_3Au(\mu_2\text{-}SC_6F_5)(AudppfAu)(\mu_2\text{-}SC_6F_5)\text{-}Au(C_6F_5)_3]$ [dppf = 1,1′-bis(diphenylphosphino)ferrocene][10] and sulfido derivatives such as $[S(AuL)_n]^{(n-2)+}$ (L = phosphine, diphosphine; $n = 2-6$)[47,48] and $[S(Au_2L_2)\{Au(C_6F_5)_3\}_n]$ ($n = 2$, L = PPh$_3$; $n = 1$, 2, L$_2$ = dppf).[8,9]

(30) We considered refining the structure of **5** in the centrosymmetric space group *Pbcn*. We were, of course, aware of the problem with space group ambiguity. We found the following. (i) In *Pbcn*, there are 987 violations of the systematic absences for the *n* glide plane. (ii) The structure can indeed be solved in *Pbcn*, but the refinement stalls at wR2 = 50%, with a large number of difference peaks of 2−4 e Å^{-3}. (iii) The basic routine ADDSYMM of the program PLATON (A.L. Spek, University of Untrecht, Netherlands) indeed suggests the higher symmetry (as we had already ascertained) but its EXACT counterpart does not, confirming the significant departure from centrosymmetry. Other symmetry-checking programs come to the same conclusion. We accept that a disordered centrosymmetric model might, in general, be better than an ordered noncentrosymmetric model but nevertheless prefer the latter in this case. Clearly, final proof becomes more difficult as the deviation from centrosymmetry becomes smaller (and least-squares matrices tend to singularity).

(31) Parr, R. G.; Yang, W. *Density Functional Theory of Atoms and Molecules*; Oxford University Press: New York, 1989.
(32) (a) *ADF2004.01*; SCM, Theoretical Chemistry, Vrije Universiteit: Amsterdam, The Netherlands; available at http://www.scm.com. (b) Te Velde, G.; Bickelhaupt, F. M.; van Gisbergen, S. J. A.; Fonseca Guerra, C.; Baerends, E. J.; Snijders, J. G.; Ziegler, T. *J. Comput. Chem.* **2001**, *22*, 931. (c) Fonseca Guerra, C.; Snijders, J. G.; Te Velde, G.; Baerends, E. J. *Theor. Chem. Acc.* **1998**, *99*, 391.
(33) Vosko, S. H.; Wilk, L.; Nusair, M. *Can. J. Phys.* **1980**, *58*, 1200.
(34) (a) Fan, L.; Ziegler, T.; *J. Chem. Phys.* **1991**, *95*, 7401. (b) Versluis, L.; Ziegler, T. *J. Chem. Phys.* **1988**, *88*, 322.
(35) Perdew, J. P.; Chevary, J. A.; Vosko, S. H.; Jackson, K. A.; Pederson, M. R.; Singh, D. J.; Fiolhais, C. *Phys. Rev.* **1992**, *B46*, 6671.
(36) van Lenthe, E.; Ehlers, A.; Baerends, E. J. *J. Chem. Phys.* **1999**, *110*, 8943.
(37) (a) van Gisbergen, S. J. A.; Groeneveld, J. A.; Rosa, A.; Snijders, J. G.; Baerends, E. J.; *J. Phys. Chem. A* **1999**, *103*, 6835. (b) Rosa, A.; Baerends, E. J.; van Gisbergen, S. J. A.; van Lenthe, E.; Groeneveld, J. A.; Snijders, J. G.; *J. Am. Chem. Soc.* **1999**, *121*, 10356. (c) van Gisbergen, S. J. A.; Rosa, A.; Ricciardi, G.; Baerends, E. J. *J. Chem. Phys.* **1999**, *111*, 2499.
(38) (a) I. Mayer. *Chem. Phys. Lett.* **1983**, *97*, 270. (b) Mayer, I. *Int. J. Quantum Chem.* **1984**, *26*, 151.
(39) Bridgeman, A. J.; Empson, C. J. *MAYER*, version 1.2.3; The University of Hull: Hull, U.K., 2004.
(40) Portmann, S.; Lüthi, H. P. *Chimia* **2000**, *54*, 766.
(41) Vicente, J.; Chicote, M. T. *Coord. Chem. Rev.* **1999**, *193*−*195*, 1143.
(42) López-de-Luzuriaga, J. M.; Sladek, A.; Schneider, W.; Schmidbaur, H. *Chem. Ber.* **1997**, *130*, 641.
(43) Vicente, J.; Chicote, M. T.; Bermudez, M. D.; Jones, P. G.; Fittschen, C.; Sheldrick, G. M. *J. Chem. Soc., Dalton Trans.* **1986**, 2361.
(44) Fackler, J. P.; Staples, R. J.; Assefa, Z. *Chem. Commun.* **1994**, 431.
(45) Usón, R.; Laguna, A.; Laguna, M.; Tarton, M. T.; Jones, P. G. *Chem. Commun.* **1988**, 740.
(46) Sladek, A.; Angermaier, K.; Schmidbaur, H. *Chem. Commun.* **1996**, 1959.
(47) Canales, F.; Gimeno, M. C.; Jones, P. G.; Laguna, A. *Angew. Chem., Int. Ed. Engl.* **1994**, *33*, 769.

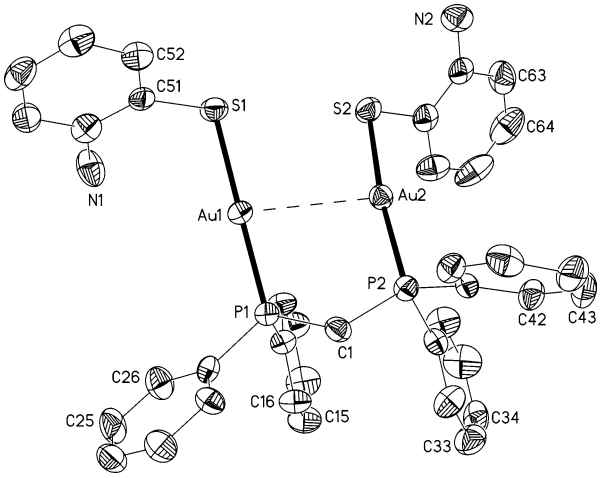

Figure 1. Structure of **3**, showing displacement ellipsoids at the 50% probability level and the atom-numbering scheme. H atoms have been omitted for clarity.

Table 2. Selected Bond Lengths (Å) and Angles (deg) for Complex **3**

Au(1)−P(1)	2.2519(17)	S(1)−C(51)	1.767(7)
Au(1)−S(1)	2.2967(17)	S(2)−C(61)	1.773(8)
Au(1)−Au(2)	3.1346(4)	N(1)−C(56)	1.369(9)
Au(2)−P(2)	2.2496(18)	N(2)−C(62)	1.374(9)
Au(2)−S(2)	2.2986(19)		
P(1)−Au(1)−S(1)	179.18(7)	P(2)−Au(2)−Au(1)	91.63(5)
P(1)−Au(1)−Au(2)	82.21(5)	S(2)−Au(2)−Au(1)	95.37(5)
S(1)−Au(1)−Au(2)	97.16(5)	C(51)−S(1)−Au(1)	105.1(2)
P(2)−Au(2)−S(2)	172.72(7)	C(61)−S(2)−Au(2)	100.7(2)

Therefore, we carried out reactions with a gold(III) derivative that led to mixed di- or tetranuclear gold(I)−gold(III) derivatives **4** and **5** according to Scheme 1.

Complexes **4** and **5** are air- and moisture-stable white (**4**) or yellow (**5**) solids at room temperature. They were readily characterized by elemental analysis and mass, IR, and NMR spectroscopies. The main features are as follows: (a) the IR spectra show absorptions around 970, 805, and 795 cm^{-1} due to the pentafluorophenyl groups;[49] (b) the ^{19}F NMR spectra show the presence of one type of tris(pentafluorophenyl)gold(III) unit; and (c) a singlet is observed in the phosphorus NMR spectra. Features b and c point to a symmetric structure for complex **5**.

X-ray Crystal Structure Determination of Derivatives 3 and 5. (i) Crystal Structure of Complex 3. The structure of the complex **3** was established by X-ray diffraction and is shown in Figure 1, with selected bond lengths and angles reported in Table 2. The angles P(1)−Au(1)−S(1) [179.18(7)°] and P(2)−Au(2)−S(2) [172.72(7)°] indicate a linear geometry around both gold atoms, although slightly distorted for Au(2). The intramolecular Au−Au distance, 3.1346(4) Å, indicates metal−metal interaction; the observed Au(1)−P(1)···P(2)−Au(2) torsion angle of −24.1° shows that the two P−Au−S moieties are slightly twisted with respect to each other; this cis conformation is usually preferred to the trans conformation, which has been observed in only a few cases, e.g., [{Au(Fmes)}$_2$(μ-dppm)] (Fmes = 2,4,6-tris(trifluoromethyl)phenyl].[50] The Au(1)−Au(2) distance is shorter than that found in the related compound [{Au(2-SPym-4-NH$_2$)}$_2$(μ-dppm)][51] [3.3317(2) Å; 2-SPym-4-NH$_2$ = 4-amino-2-pyrimidinethiol], but longer than those in [{Au(SSNH$_2$)}$_2$(μ-dppm)][52] [3.0987(10) Å; SSNH$_2^-$ = 2-amino-5-mercapto-1,3,4-thiadiazolate] and [{Au(dpt)}$_2$(μ-dppm)][53] [3.0353(3) Å; dpt = S$_2$P(*p*-C$_6$H$_4$OMe)(O-*c*-C$_5$H$_9$)], all of which contain a single dppm bridge. There are no short gold−gold intermolecular contacts.

Table 3. Hydrogen Bonds for Complex **3** (Å and deg)

D−H···A[a]	*d*(D−H)	*d*(H···A)	*d*(D···A)	<(DHA)
N(1)−H(1B)···S(2) #1	0.89	2.67	3.507(7)	158.3
N(2)−H(2B)···S(1) #2	0.89	2.65	3.537(7)	178.8

[a] Symmetry transformations used to generate equivalent atoms: #1 −*x*, −*y* + 2, −*z*; #2 −*x*, −*y* + 1, −*z*.

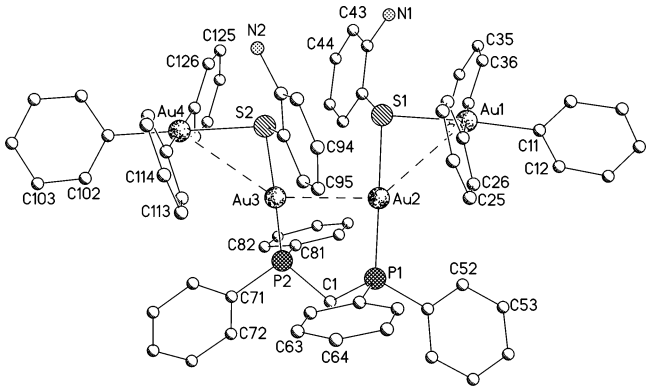

Figure 2. Structure of one of the two independent molecules of complex **5** in the crystal. H and F atoms have been omitted for clarity. Radii are arbitrary.

The Au−P [2.2496(18), 2.2519(17) Å] and Au−S [2.2967(17), 2.2986(19) Å] bond distances are typical for this type of complex. Complex **3** also shows two N−H···S contacts that can be interpreted as hydrogen bonds (Table 3).

(ii) Crystal Structure of Complex 5. The tetranuclear structure of **5** was confirmed by X-ray diffraction studies; it crystallizes with two independent molecules and disordered solvent in the asymmetric unit. One molecule is shown in Figure 2, and a selection of bond lengths and angles is collected in Table 4.

As expected, the coordination geometries of the Au^{I} and Au^{III} centers are linear and square-planar, respectively, with only slight distortions. After complexation of the gold(III) fragments, there is a shortening of the gold(I)−gold(I) distance to 2.9353(7) Å [2.9332(7) Å in the second molecule], which has not been observed in other similar mixed complexes. To our knowledge, this Au^{I}−Au^{I} bond length is the shortest reported for a monobridged dinuclear dppm gold complex. The Au(2)−P(1)···P(2)−Au(3) torsion angle of −35.4(1)° [34.0(1)°], therefore shows the usual cis confor-

(48) Canales, F.; Gimeno, M. C.; Laguna, A.; Jones, P. G. *J. Am. Chem. Soc.* **1996**, *118*, 4839.
(49) Usón, R.; Laguna, A.; García, J.; Laguna, M. *Inorg. Chim. Acta* **1979**, *37*, 201.
(50) Bardají, M.; Jones, P. G.; Laguna, A.; Moracho, A.; Fischer, A. K. *J. Organomet. Chem.* **2002**, *648*, 1.
(51) Wilton-Ely, J. D. E. T.; Schier, A.; Mitzel, N. W.; Nogai, S.; Schmidbaur, H. *J. Organomet. Chem.* **2002**, *643*−*644*, 313.
(52) Tzeng, B.; Schier, A.; Schmidbaur, H. *Inorg. Chem.* **1999**, *38*, 3978.
(53) Maspero, A.; Kani, I.; Mohamed, A. A.; Omary, M. A.; Staples, R. J.; Fackler, J. P., Jr. *Inorg. Chem.* **2003**, *42*, 5311.

Table 4. Selected Bond Lengths (Å) and Angles (deg) for Complex **5**[a]

Au(1)−C(31)	2.001(14)	Au(1′)−C(131)	2.036(13)
Au(1)−C(11)	2.050(13)	Au(1′)−C(151)	2.064(13)
Au(1)−C(21)	2.071(13)	Au(1′)−C(141)	2.091(15)
Au(1)−S(1)	2.375(3)	Au(1′)−S(1′)	2.372(3)
Au(1)−Au(2)	3.2812(7)	Au(1′)−Au(2′)	3.2923(7)
Au(2)−P(1)	2.269(3)	Au(2′)−P(1′)	2.268(3)
Au(2)−S(1)	2.341(3)	Au(2′)−S(1′)	2.342(3)
Au(2)−Au(3)	2.9353(7)	Au(2′)−Au(3′)	2.9332(7)
Au(3)−P(2)	2.270(3)	Au(3′)−P(2′)	2.271(3)
Au(3)−S(2)	2.332(3)	Au(3′)−S(2′)	2.337(3)
Au(3)−Au(4)	3.3822(7)	Au(3′)−Au(4′)	3.4052(7)
Au(4)−C(111)	2.017(14)	Au(4′)−C(231)	2.036(14)
Au(4)−C(101)	2.039(15)	Au(4′)−C(221)	2.044(14)
Au(4)−C(121)	2.105(15)	Au(4′)−C(241)	2.081(15)
Au(4)−S(2)	2.372(3)	Au(4′)−S(2′)	2.375(3)
C(31)−Au(1)−C(11)	91.2(4)	C(131)−Au(1′)−C(151)	89.8(4)
C(31)−Au(1)−C(21)	177.6(4)	C(131)−Au(1′)−C(141)	91.4(4)
C(11)−Au(1)−C(21)	90.1(4)	C(151)−Au(1′)−C(141)	177.0(4)
C(31)−Au(1)−S(1)	93.2(3)	C(131)−Au(1′)−S(1′)	174.0(3)
C(11)−Au(1)−S(1)	175.0(3)	C(151)−Au(1′)−S(1′)	85.3(3)
C(21)−Au(1)−S(1)	85.6(3)	C(141)−Au(1′)−S(1′)	93.7(3)
C(31)−Au(1)−Au(2)	102.5(3)	C(131)−Au(1′)−Au(2′)	130.2(3)
C(11)−Au(1)−Au(2)	131.0(3)	C(151)−Au(1′)−Au(2′)	78.2(3)
C(21)−Au(1)−Au(2)	78.1(3)	C(141)−Au(1′)−Au(2′)	103.0(3)
S(1)−Au(1)−Au(2)	45.48(7)	S(1′)−Au(1′)−Au(2′)	45.33(7)
P(1)−Au(2)−S(1)	174.47(13)	P(1′)−Au(2′)−S(1′)	174.28(14)
P(1)−Au(2)−Au(3)	87.89(9)	P(1′)−Au(2′)−Au(3′)	87.24(9)
S(1)−Au(2)−Au(3)	91.92(8)	S(1′)−Au(2′)−Au(3′)	93.53(8)
P(1)−Au(2)−Au(1)	133.79(10)	P(1′)−Au(2′)−Au(1′)	133.34(9)
S(1)−Au(2)−Au(1)	46.33(8)	S(1′)−Au(2′)−Au(1′)	46.09(8)
Au(3)−Au(2)−Au(1)	138.22(2)	Au(3′)−Au(2′)−Au(1′)	139.41(2)
P(2)−Au(3)−S(2)	176.23(13)	P(2′)−Au(3′)−S(2′)	177.66(13)
P(2)−Au(3)−Au(2)	88.00(9)	P(2′)−Au(3′)−Au(2′)	89.56(9)
S(2)−Au(3)−Au(2)	94.30(8)	S(2′)−Au(3′)−Au(2′)	92.40(8)
C(111)−Au(4)−C(101)	91.6(5)	C(231)−Au(4′)−C(221)	91.9(4)
C(111)−Au(4)−C(121)	176.4(4)	C(231)−Au(4′)−C(241)	177.6(4)
C(101)−Au(4)−C(121)	90.8(5)	C(221)−Au(4′)−C(241)	89.6(5)
C(111)−Au(4)−S(2)	93.1(3)	C(231)−Au(4′)−S(2′)	84.9(3)
C(101)−Au(4)−S(2)	175.0(4)	C(221)−Au(4′)−S(2′)	176.4(3)
C(121)−Au(4)−S(2)	84.6(3)	C(241)−Au(4′)−S(2′)	93.7(3)
Au(2)−S(1)−Au(1)	88.19(10)	Au(2′)−S(1′)−Au(1′)	88.58(10)
Au(3)−S(2)−Au(4)	91.93(11)	Au(3′)−S(2′)−Au(4′)	92.53(11)

[a] Primes indicate atoms of the second independent molecule.

mation. The $Au^{I}-Au^{III}$ distances, 3.2812(7) and 3.3822(7) Å [3.2923(7) and 3.4052(7) Å], are comparable to those obtained for the complex $[\{S(Au_2dppf)\}_2\{Au(C_6F_5)_2\}][CF_3SO_3]$ [3.2195(8), 3.3661(10) Å][9] with a bridging sulfide ligand, but shorter than those reported in other sulfide, thiolate, or selenide mixed derivatives [3.404(1) − 4.011(1) Å].[8−11] The shortest of these $Au^{I}-Au^{III}$ distances are similar to the $Au^{I}-Au^{I}$ contacts in many molecules. The Au−S−Au angles differ slightly, with the narrower, 88.19(10)° [Au(1)−S(1)−Au(2)] [88.58(10)°], corresponding to the shortest $Au^{I}-Au^{III}$ distance.

A lengthening of the $Au^{I}-S$ distances should be expected as a consequence of the coordination of the $Au(C_6F_5)_3$ moieties; in fact, the $Au^{I}-S$ distances in **5** are 2.332(3) and 2.341(3) Å [2.337(3) and 2.342(3) Å], longer than the corresponding distances in **3**, 2.2967(17) and 2.2986(19) Å. The $Au^{III}-S$ distances of 2.372(3) and 2.375(3) Å [2.372(3) and 2.375(3) Å] compare well with those found in the mixed $Au^{I}-Au^{III}$ derivative with a bridging thiolate ligand $[(C_6F_5)_3Au(\mu_2\text{-}SC_6F_5)(AudppfAu)(\mu_2\text{-}SC_6F_5)Au(C_6F_5)_3]$.[10] The Au−P lengths are similar to those observed in **3**.

Photophysical Studies. The absorption spectra of these complexes and the ligands were measured in the range 200−600 nm, and the results are summarized in Table 5. The

Table 5. Electronic Absorption Data for the Thiol and Complexes **1**−**5**[a]

compd	λ/nm (ε × 10^{-3}/M^{-1} cm^{-1})
$HSC_6H_4NH_2$	247 sh (6.5), 300 (2.3), 349 sh (0.3)
1	245 sh (32), 269 sh (11), 277 sh (8.2), 311 (6.2)
2	268 (34), 274 (30), 319 (21)
3	266 sh (16), 277 sh (13), 308 sh (5.5)
4	244 sh (33), 269 (18), 276 (17), 345 (5.2)
5	268 sh (41), 277 (42), 342 (9.4)

[a] In CH_2Cl_2 solution, 5.0×10^{-5} M.

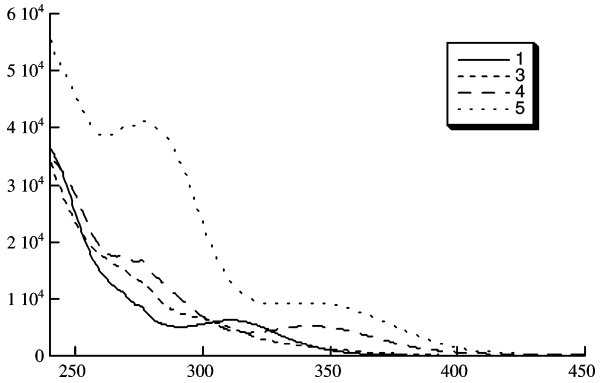

Figure 3. UV−vis absorption spectra of complexes **1** and **3**−**5** (ε in M^{-1} cm^{-1} versus wavelength in nm).

spectra of complexes **1** and **3**−**5** are shown in Figure 3. The absorptions below 300 nm are related to the pentafluorophenyl, phosphine, or thiol ligands; the addition of the gold(III) fragments to complexes **1** or **3** increases the intensity of the absorptions around 270 and 280 nm. The lowest-energy band, absent in the chloro analogues $[AuCl(PPh_3)]$ and $[(AuCl)_2(\mu\text{-dppm})]$, has usually been related to sulfur-to-gold charge-transfer transitions and shifts from ca. 310 to ca. 340 nm after coordination of gold(III) to sulfur.[18,23,54] Accordingly, these peaks are tentatively assigned to ligand-to-metal [gold(III) and/or gold(I)] charge-transfer transitions, although the thiol ligand shows a weak absorption in this region. In addition, there are absorption tails that extend to ca. 360 nm (derivatives **1** and **2**), ca. 380 nm (derivative **3**), ca. 410 nm (derivative **4**), and ca. 425 nm (derivative **5**). Further discussion of these assignments is provided in conjunction with the discussion of the computational results below.

The solid-state emission and excitation spectra at 77 K for the isolated complexes were obtained and are shown in Figure 4. The compounds do not emit at room temperature. In this case, the most striking feature is the intense photoluminescence at 77 K, with emission maxima at 452 (**1**), 465 (**2**), and 538 (**3**) nm for the gold(I) thiolate complexes, whereas the mixed gold(I)−gold(III) thiolate derivatives are not emissive. The excitation spectra are complex, with maxima at 330 (**1**), 353 (**2**), and 391 (**3**) nm. Compound **3** shows the broadest emission peak, and a second, less intense emission peak centered at 514 nm can be obtained, with an excitation maximum at 359 nm.

The emission observed in gold(I) thiolate complexes has usually been assigned as arising from a S (π)-to-Au (6p) LMCT excited state and is therefore affected by the substituents of the thiolate ligand.[12,54] When substituents on the thiolate do not produce significant electronic perturbations,

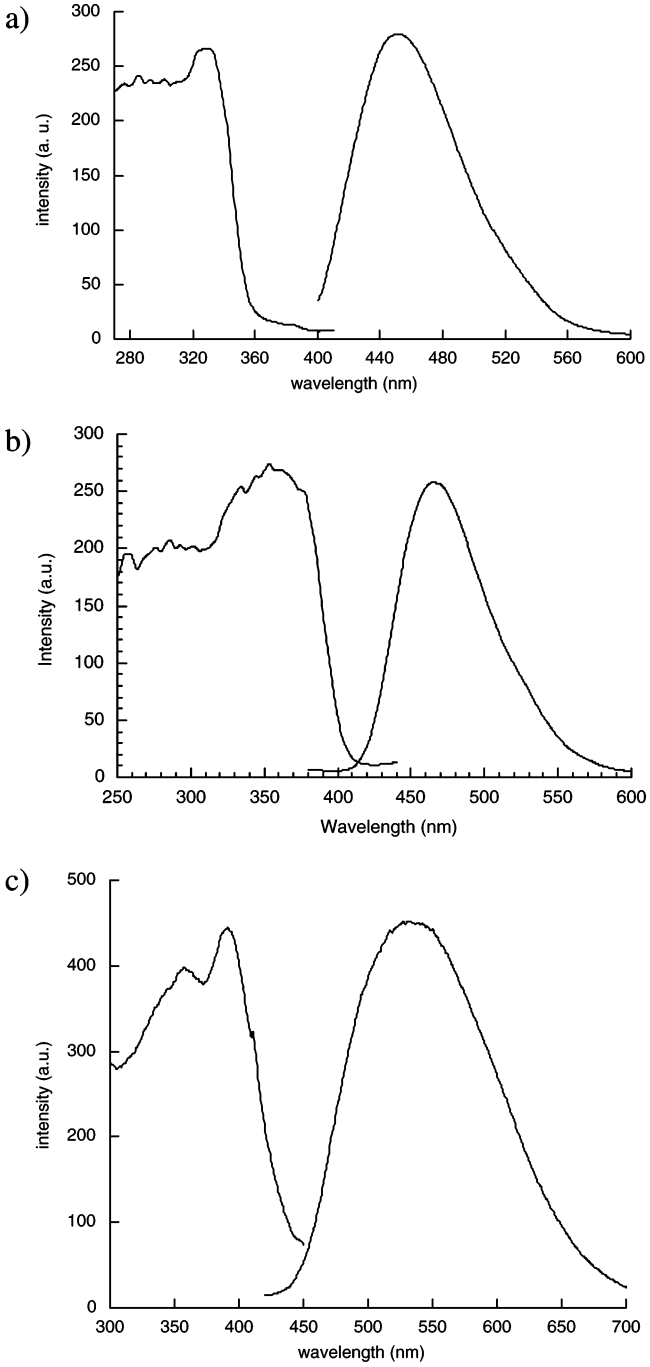

Figure 4. Excitation and emission spectra at 77 K in the solid state: (a) complex **1**, (b) complex **2**, (c) complex **3**.

the presence of gold−gold interactions strongly influences the emission bands, which become LMMCT in nature.[13−15,55] The shift of the emission maxima in a series of substituted benzenethiolate derivatives has suggested an MLCT transition.[21] Moreover, the existence of π electrons in the phosphine ligand can complicate the assignment because an LLCT transition [S (π) to Ph (π^*)] is possible.[21] LC transitions can also contribute to the emission spectra when selected ligands are used.[15,56] Finally, multiple state emissions (MC, LMCT, and LMMCT) have been proposed to explain the white emission and the thermochromism of dialkyldithiophosphonate dinuclear derivatives.[57]

Table 6. Relevant Calculated Distances (Å) and Angles (deg) for Models of Complexes **1**−**3**, Compared with Experimental Values for **3**

distance/angle	**3**[a]	**3h**	**3m**	**2**	**1**	**1h**	**1m**
Au···Au	3.135	3.142	3.197	−	−	−	−
Au−S	2.297	2.418	2.317	2.315	2.319	2.314	2.320
	2.299	2.428	2.319	2.330			
Au−P	2.250	2.424	2.271	−	2.298	2.265	2.278
	2.253	2.431	2.277				
Au···N	3.497	3.597	3.609	3.258	3.601	3.537	3.530
	4.792	4.872	4.836	3.865			
P−C (dppm)	1.841	1.858	1.855	−	−	−	−
	1.846		1.856				
S−Au−P	173	172	172	−	175	178	177
	179	178	179				
S−Au−S	−	−	−	174	−	−	−
Au−P···P−Au	24.1	27.0	25.9	−	−	−	−

[a] X-ray structure.

X-ray diffraction studies showed that the nonemissive tetranuclear gold(I)−gold(III) thiolate complex **5** exhibits a shorter gold(I)−gold(I) distance than the strongly emissive parent dinuclear gold(I) thiolate complex **3**. A purely metal−metal-centered transition should thus be ruled out. The spectrum of complex **3** is red-shifted compared to that of complex **1**, a typical behavior induced by the gold(I)−gold(I) interactions, which points to an LMCT transition (or an LMMCT transition for the emission of complex **3**). The same assignment could explain why complexes **4** and **5** are nonemissive: After coordination of the gold(III) fragment, the latter transition becomes less likely, and other transitions involving the gold(III) center could take place. TD-DFT calculations should help to clarify the nature of these transitions.

DFT Calculations. DFT calculations (ADF program; see details in the Experimental Section) were performed to elucidate the nature of the bonding in these complexes and to interpret the optical properties of the gold(I) and gold(I)−gold(III) complexes described above. The phenyl groups of the phosphine ligands are modeled by hydrogen (**h** models) or by a methyl group (**m** models), and C_6F_5 is modeled by CF_3, owing to the size of some of the complexes, especially complex **5** with four gold atoms and several ligands. The models of each complex are denoted as **1h**, **1m**, **3h**, **3m**, **4h**, and **5h**. Complexes **1** and **2** were also fully calculated.

(i) Au(I) Complexes. The quality of the models was checked by comparing the geometries of models **3h** and **3m** with the experimental data for complex **3**. Some relevant distances and angles are given in Table 6.

DFT methods provide good agreement between experimental and calculated structures, except when weak interactions, such as the Au(I)···Au(I) interaction in complex **3**, exist. Again, the size of the systems prevented us from using

(54) Narayanaswamy, R.; Young, M. A.; Parkhurst, E.; Ouellette, M.; Kerr, M. E.; Ho, D. M.; Elder, R. C.; Bruce, A. E.; Bruce, M. R. M. *Inorg. Chem.* **1993**, *32*, 2506.
(55) Roundhill, D. M.; Fackler, J. P., Jr. *Optoelectronic Properties of Inorganic Compounds*; Plenum Press: New York, 1998; p 195.
(56) Van Zyl, W. E.; López-de-Luzuriaga, J. M.; Mohamed, A. A.; J. M.; Staples, R. J.; Fackler, J. P., Jr. *Inorg. Chem.* **2002**, *41*, 4579.
(57) Lee, Y. A.; McGarrah, J. E.; Lachicotte, R. J.; Eisenberg, R. *J. Am. Chem. Soc.* **2002**, *124*, 10662.

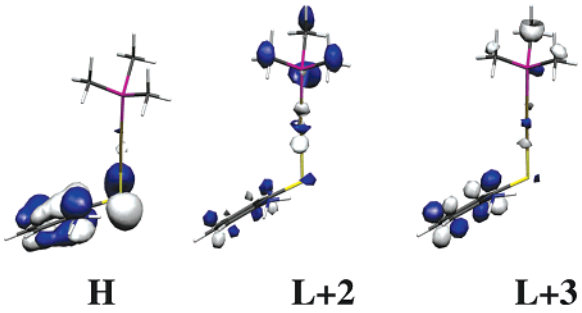

Figure 5. Representation of the orbitals of model **1m** of complex [Au(2-$SC_6H_4NH_2$)(PPh_3)] (**1**) involved in the lowest-energy transition.

more suitable correlated methods. The calculated values 3.142 and 3.197 Å for models **3h** and **3m**, respectively, compare surprisingly well with the experimental Au−Au distance of 3.135 Å, as do the P−C distances and the angles. On the other hand, the Au−S and Au−P distances in **3h** are too long. The introduction of the methyl groups leads to a better agreement between calculated and experimental values in the Au−S and Au−P distances. Mayer indices (MIs), which measure the bond strengths independently of the distance, indicate a stronger Au···Au bond (MI = 0.187) for **3m** than for **3h** (0.138). In complex **1**, the introduction of phenyl groups lengthens the Au−P bond by ca. 0.03 Å, the other distances and angles remaining the same. Although both **1h** and **1m** provide a good model for complex **1**, methyl groups must be included (**3m**) to obtain a good model of complex **3**.

The energy, composition, and nature of the frontier orbitals of models **1h** and **1m** and complex **1** are given in the Supporting Information. TD-DFT calculations were performed in order to assign the absorption spectra (see Supporting Information). The lower-energy absorptions should correspond to the excitation maxima observed in the solid state at 77 K and be responsible for the luminescent properties.

For complex **1**, the agreement between the calculated and experimental (311 nm; UV−vis spectrum) values is better when PMe_3 (316 nm, **1m**), rather than PH_3 (293 nm, **1h**), is used in the model. This band is assigned to a mixed transition from the HOMO to LUMO+2 (62%) and LUMO+3 (17%), the HOMO being a thiolate-based orbital (88% thiolate, with 25% in sulfur) and the LUMOs being strongly located on the phosphine, with a large contribution of gold. The transition can thus be assigned as LMCT (S → Au−P charge transfer) with some mixture of LLCT. The three orbitals involved are shown in Figure 5.

In complex 2, the phosphine ligand of **1** has been replaced by another thiolate, so that the complex becomes anionic. The most intense calculated excitations correspond well with the experimental excitation maximum, that is, the band at 353 nm is calculated to appear at 359 nm, with the shoulder at 335 nm being reproduced by the two bands at 343 and 330 nm. The experimental band at 319 nm in the UV−vis absorption spectrum is also close to the calculated value (359 nm), especially taking into account that the species is anionic and solvent effects should be more important in this case.

The transition at 359 nm results from mixed excitations from the HOMO to LUMO+1 (22%), LUMO+2 (19%), and LUMO+3 (32%). The HOMO is 80% located on the thiolate (49% on sulfur), whereas the three LUMOs are located on one of the thiolates (Figure 6). Gold does not contribute more than 10% to each orbital. Therefore, the excitations can be assigned as interligand, from S in one ligand to the π^* levels of the other (LUMO+2, LUMO+3), or intraligand, from S to π^* in the same ligand (LUMO+1). The excitation can be assigned to LLCT (S → π^*) mixed with ILCT. The introduction of the second thiolate changes the character of the low-energy transitions.

3m was found to be a better model for complex **3** than **3h**. The details on the frontier orbitals are given in the Supporting Information. These complexes have two gold atoms, being close to a dimer of complex **1**. The same trends are observed, that is, the occupied levels are strongly localized on the thiolate ligand (and mostly on sulfur) whereas the empty ones show participation of the metal and the phosphine ligand.

The agreement between the TD results (**3m**) and those experimentally obtained for complex **3** is quite good. The most intense transitions are calculated at 322 and 345 nm for **3m**, the experimental value for absorption being 308 nm. These transitions start in HOMO−5 and HOMO−4, and both end in the LUMO. There is no relevant mixing of other transitions. HOMO−5 and HOMO−4, as well as the HOMO and other orbitals between them, are essentially located on one or both of the thiolate ligands, with different contributions of sulfur and the π levels of the phenyl group (Figure 7). The LUMO is located on the two gold(I) atoms and the phosphorus (Figure 7), representing the Au···Au interaction and the Au−P bond.

These transitions can therefore be assigned to LMCT (S → Au···Au−P charge transfer), mixed with some LLCT and MC character. A similar result was obtained for the complex [Au_2(μ-i-mnt)(μ-dppm)], in which the low-energy absorption is a combination of S (p_y) → dppm, S (p_y) → Au (p_z) and Au($d_{x^2-y^2}$) → Au (p_z).[25] This assignment is similar to that obtained for the model of **1** (**1m**), LMCT (S → Au−P), but the gold atom is also involved in the Au−Au interaction. The transition energies are shifted, and the nature of the transition is modified to include the Au···Au interaction.

(ii) Au(III) Complexes. The mixed Au(I)−Au(III) complexes **4** and **5** contain one or two additional Au(C_6F_5)$_3$ units bound to the sulfur atoms, compared to **1** and **3**. The crystal structure of **5** revealed a significant contraction of the Au···Au distance to 2.935 Å, compared to that in **3**, which was the most interesting structural aspect introduced by binding of the gold(III) fragments. Although the calculated gold(I)−gold(I) distance (3.294 Å) is longer than in **3h** (3.142 Å) and much longer that the experimental value (2.935 Å), the MIs indicate that the Au···Au interaction is stronger in **5h** (0.142) than in **3h** (0.138). We already pointed out the limitations of model **3h**, so model **5h** should also provide only moderate agreement with experiment.

The composition of the frontier orbitals of model **4h** (see the Supporting Information) differs from what was found

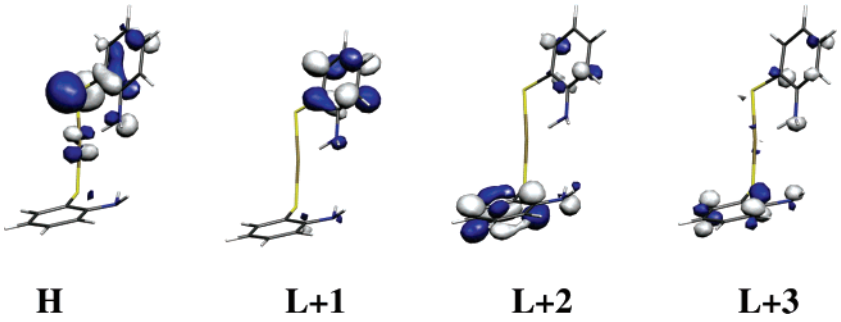

Figure 6. Representation of the orbitals of complex $[Au(2\text{-}SC_6H_4NH_2)_2]^-$ (**2**) involved in the lowest-energy transition.

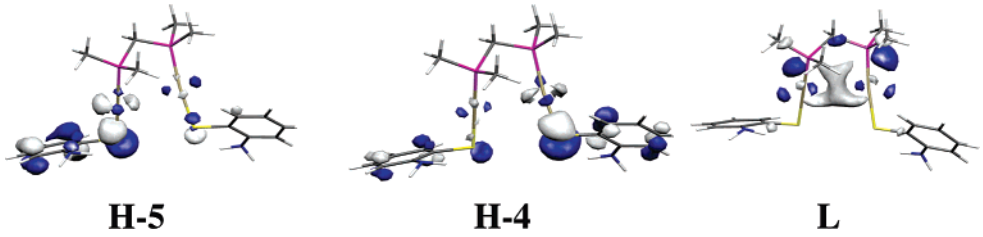

Figure 7. Representation of the orbitals of model **3m** of complex $[\{Au(2\text{-}SC_6H_4NH_2)\}_2(\mu\text{-dppm})]$ (**3**) involved in the lowest-energy transition.

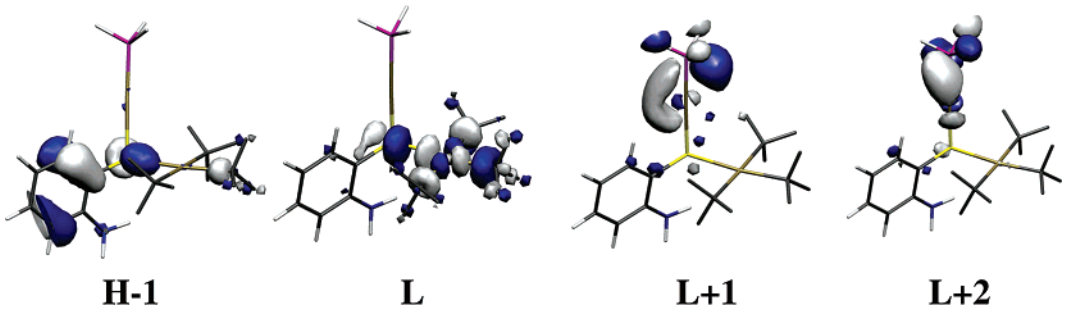

Figure 8. Representation of the orbitals of model **4h** of complex $[(AuPPh_3)\{Au(C_6F_5)_3\}(\mu_2\text{-}2\text{-}SC_6H_4NH_2)]$ (**4**) involved in the lowest-energy transition.

for complexes **1**−**3**, as the Au(III) fragment participates to a significant extent in many of them. The two most intense excitations were calculated at 345 and 319 nm, in agreement with the experimental values (345 nm for absorption). The first transition has two components, both starting at HOMO−1 and ending at the LUMO (61%) or LUMO+1 (27%); the two components of the second transition also start at HOMO−1, ending at LUMO+2 (75%) or the LUMO (11%). HOMO−1 is 82% located on the thiolate ligand, but the sulfur atom contributes much less to it than in the related **1m** model complex, the π levels of the phenyl group being more important. The LUMO is 69% localized in the Au(III)−$(CF_3)_3$ fragment (26% in gold), whereas LUMO+1 and LUMO+2 are Au(I)−P σ* levels (ca. 60% on the phosphine and ca. 20% on gold). These four levels are shown in Figure 8.

The experimental absorption around 350 nm in the absorption spectrum should arise from a mixed LMCT (thiolate → Au^{III} and thiolate → Au−P). The strong involvement of Au(III) in the LUMO changes the character of the excited state and most probably influences the emissive state. Notice that the sulfur atom is absent in the levels associated with the excitations, whereas it played an important role in the mononuclear Au(I) complex.

The most intense excitations calculated for complex **5h** (Supporting Information) are similar in nature to those found for **4h**, but their quality is limited by the same factors as for model complex **3h**. It can still be stated, however, that the lowest excitations also start on π* orbitals of the phenyl group in the thiolate ligand and end on combinations of Au(III) d and Au(I)−P σ* orbitals. Significant shifts are found between the calculated (448 nm) and experimental (342 nm) values. The use of H instead of Ph influences the calculated energies because it also affects the Au···Au interactions, which seems to be important for these transitions, as seen for model complex **3h**. Also, all of the calculations are limited by the quality of the DFT method.

Conclusions

The acac method is well suited to the preparation of phosphino gold(I) derivatives **1**−**3** of 2-aminobenzenethiolate, which emit intensely in the solid state at 77 K. The sulfur atoms are able to coordinate to $Au(C_6F_5)_3$ moieties to give di- and tetranuclear mixed gold(I)−gold(III) derivatives **4** and **5**; the latter shows a shortening of the intramolecular gold(I)−gold(I) interaction (already observed in **3**) and short gold(I)−gold(IIII) distances. This coordination to the thiolate ligand of a strongly electron-withdrawing gold(III) fragment quenches the emission. DFT studies allowed us to determine the electronic levels of these derivatives, and TD-DFT calculations allowed us to determine the electronic excitations. The excitation transitions could thus be mainly

assigned (all are mixtures) as LMCT (S→ Au−P charge transfer) for derivative **1**, LLCT for derivative **2**, and LMMCT (S→ Au···Au−P charge transfer) for derivative **3**. The introduction of Au(III) in the structure results in the appearance of thiolate → Au^{III} transitions for derivatives **4** and **5**. The change in the character of the absorbing state probably affects the way the complex reaches the emissive state and leads to the quenching of luminescence.

Acknowledgment. This work is dedicated to Dr. José Antonio Abad on the occasion of his retirement. We thank the Dirección General de Investigación Científica y Técnica (Project BQU2001-2409-C02-01) and the Fonds der Chemischen Industrie for financial support. We thank Acção Integrada Luso-Espanhola E31/04. P.J.C. acknowledges FCT for a grant (SFRH/BD/10535/2002).

Supporting Information Available: Structural data for **3** and **5** (CIF format); tables of population analyses of **1h**, **1m**, **1**, **2**, **3h**, **3m**, **4h**, and **5h**; tables of calculated excitations and oscillator strengths of **1h**, **1m**, **1**, **2**, **3h**, **3m**, **4h**, and **5h**; relevant calculated distances and angles for models of complexes **4h** and **5h**, compared to experimental values for **5**; representations of the frontier orbitals of **1**. This material is available free of charge via the Internet at http://pubs.acs.org.

IC051168U